Stability of the I-motif Structure Is Related to the Interactions between Phosphodiester Backbones

Thérèse E. Malliavin,* Jocelyne Gau,* Karim Snoussi,[†] and Jean-Louis Leroy[‡]

*Laboratoire de Biochimie Théorique, Centre National de la Recherche Scientifique, Institut de Biologie Physico-Chimique, Paris, France; [†]Department of Biophysical Chemistry, Lund University, Lund, Sweden; and [‡]Laboratoire de RMN à Haut Champ ICSN-Centre National de la Recherche Scientifique, Gif-sur-Yvette, France

ABSTRACT   The i-motif DNA tetrameric structure is formed of two parallel duplexes intercalated in a head-to-tail orientation, and held together by hemiprotonated cytosine pairs. The four phosphodiester backbones forming the structure define two narrow and wide grooves. The short interphosphate distances across the narrow groove induce a strong repulsion which should destabilize the tetramer. To investigate this point, molecular dynamics simulations were run on the [d(C2)]4 and [d(C4)]4 tetramers in 3′E and 5′E topologies, for which the interaction of the phosphodiester backbones through the narrow groove is different. The analysis of the simulations, using the Molecular Mechanics Generalized Born Solvation Area and Molecular Mechanics Poisson-Boltzmann Solvation Area approaches, shows that it is the van der Waals energy contribution which displays the largest relative difference between the two topologies. The comparison of the solvent-accessible area of each topology reveals that the sugar-sugar interactions account for the greater stability of the 3′E topology. This stresses the importance of the sugar-sugar contacts across the narrow groove which, enforcing the optimal backbone twisting, are essential to the base stacking and the i-motif stability. Tighter interactions between the sugars are observed in the case of N-type sugar puckers.

INTRODUCTION

The tetrameric DNA structures (Keniry, 2000; Guéron and Leroy, 2000) are thought to play an important role in chromatin organization in the cell nucleus (Arthanari and Bolton, 2001). Two main types of tetrameric structures are known: the G-quartets (Keniry, 2000) observed in G-rich sequences, and the i-motif (Gehring et al., 1993), formed by the antiparallel intercalation of two C-rich parallel duplexes. Centromeric (Nonin-Lecomte and Leroy, 2001) and telomeric (Ahmed et al., 1994; Phan et al., 2000) DNA sequences were shown in vitro to be folded into i-motif structures. The i-motif is built by the intercalation of two parallel duplexes, forming a rectangular-shaped structure, in which the positions of the four phosphodiester backbones define a wide and a narrow groove.

The structural bases of the i-motif stability are not fully understood. Indeed, a strong repulsive interaction exists between the charged C-imino protons (estimated to be 65 kcal/mol; Spóner et al., 1996), and between the phosphate groups across the narrow groove. On the other hand, attractive interactions are observed between C/C+ pairs, which were estimated to be −32 kcal/mol for ion-dipole and stacking (Spóner et al., 1996) and −14.1 to −19.1 kcal/mol for Lennard-Jones (Gallego et al., 1999). Attractive interactions are also expected between C4–N4 and C2–O2 dipoles of stacked C/C+ pairs, which are nearly antiparallel in the i-motif structures (Gallego et al., 1999), and between the N3 and H3+ atoms of the cytosines forming a hemiprotonated C/C+ pair (−45 kcal/mol; Spóner et al., 1996). The sum of all attractive interactions between the bases can thus compensate for the C-imino proton repulsion, as observed in the nanosecond molecular dynamics simulations of the i-motif (Spackóva et al., 1998). However, this energy balance does not account for the different widths of the i-motif grooves, and for the subsequent repulsion of phosphate groups, which are only 6 Å apart.

Concerning this last point, several conflicting observations were reported. First, Berger et al. (1996) showed that, in the x-ray crystallographic structure of [d(C4)]4, the distances and the angles between the atom O4′ and the atoms C4′ and C1′ of the sugars located on each side of the narrow groove are consistent with the existence of interstrand CH...O hydrogen bonds, which would compensate the electrostatic repulsion between the phosphate groups. But, a systematic study of the [d(Cn)]4 (n = 3–6) complexes (Leroy et al., 2001) permitted estimating the energy of a CH...O hydrogen bond as 0.6 kcal/mol, which seems too weak to balance the phosphate repulsion.

This study of [d(Cn)]4 (Leroy et al., 2001) took advantage of the existence of two topologies for the i-motif structure —one with outermost 3′ extremities and the other with outermost 5′ extremities, called, respectively, 3′E and 5′E topologies (Phan and Leroy, 2000; Leroy and Guéron, 1995). The main difference between the two topologies is the relative positions of the neighboring phosphodiester backbones, separated by the narrow grooves (Fig. 1). Indeed, because of the asymmetric position of the phosphate group between two bases, the phosphate pairs and, consequently, the sugar pairs can be grouped as close and remote pairs. Close phosphate pairs display larger electrostatic repulsion, whereas attractive interaction (due to CH...O hydrogen bonds or to another reason) are only expected for close sugar pairs. The 3′E topology exhibits an additional close phosphate pair and an
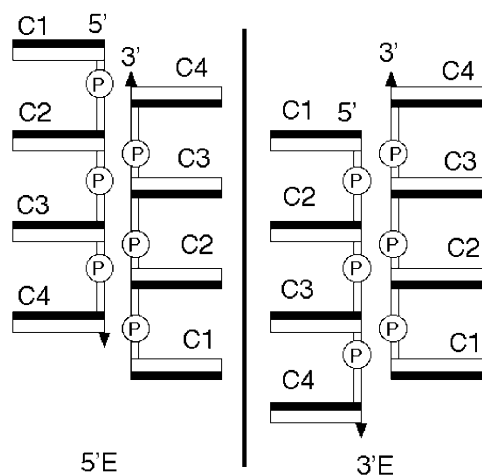
FIGURE 1 Schematic representation of the two maximally intercalated topologies 3′E and 5′E of [d(C4)]4. The scheme shows two strands on either side of a narrow groove. The bases are represented by rectangles with their black faces oriented in the 5′ direction and their white faces in the 3′ direction. The crystal structure of [d(C4)]4 adopts the 5′E topology. In solution, both topologies coexist in comparable proportions.

additional close sugar pair as compared to the 5′E topology (Fig. 1). If the balance of attractive and repulsive interactions between sugars and phosphates determine the i-motif topology, the relative stability of the 3′E and 5′E species of [d(Cn)]4 should thus not depend on n. It is observed that the two species exhibit similar stability (Leroy et al., 2001) for 3 ≤ n < 6, but, at higher ionic strength, when the phosphate-phosphate interaction is screened by Na⁺, the 3′E species is much more stable than the 5′E. In the case of [d(C2)]4, only the 3′E species is observed in solution at low ionic strength. The behaviors of [d(C2)]4 and of [d(Cn)]4 (3 ≤ n < 6) are thus opposite.

The narrow groove in the NMR structure of the [d(C2)]4 (Malliavin et al., 2003) is slightly narrower than that of the other i-motif structures. This feature, which may enhance the interaction between the neighboring phosphodiester backbones, could explain the different behavior of [d(C2)]4. Molecular dynamics (MD) simulations were run (Malliavin et al., 2003) on [d(C2)]4 and [d(C4)]4 in the two topologies, to further investigate the reasons for the difference of behavior between these tetramers. The analysis of the mean conformers from these simulations revealed that the four phosphodiester backbones must be twisted in the same way to maximize the attractive Lennard-Jones, ion-dipole, and stacking interactions between the C/C+ pairs, balancing the electrostatic repulsion between charged C-imino protons. It is likely that an attractive interaction between phosphodiester backbones is required to enforce the same helical twist, and a good candidate is the sugar-sugar interaction.

To clarify the interactions between different regions of the i-motif structure during the MD simulations run on the 3′E and 5′E topologies of [d(C2)]4 and [d(C4)]4 tetramers, we are here using the Molecular Mechanics Generalized Born

Solvation Area (MMGBSA) (Srinivasan et al., 1998), and the Molecular Mechanics Poisson-Boltzmann Solvation Area (MMPBSA) (Massova and Kollman, 1999) protocols along with an estimation of the conformational entropy of the solute (Schlitter, 1993) on the MD trajectories run on the [d(C2)]4 and [d(C4)]4 tetramers. The components of the total free energy calculated from the different simulations are analyzed, and the fit between the conformations of the neighboring phosphodiester backbones is compared according to the topology and to the sugar pucker phases.

MATERIALS AND METHODS

Molecular dynamics simulations

The starting conformations for the simulations were generated in the following way. Hydrogens were added to the 5′E topology of the [d(C4)]4 crystallographic structure (Chen et al., 1994) (PDB id: 190d), and this structure was the starting point for the MD simulations of the 5′E topology of [d(C4)]4. The model for [d(C2)]4 in 3′E topology was the structure derived from its Résonance Magnétique Nucléaire (NMR) study (Malliavin et al., 2003) (PDB id: 1M6A and RCSB id: RCSB016651). The 3′E topology of [d(C4)]4 and the 5′E topology of [d(C2)]4 were built from the other topology by translating one duplex by 6.0 Å with respect to the other along the vector perpendicular to the base planes.

The cytosine protonation was modeled by adding an H3 hydrogen to the N3 atom. One cytosine in each base pair was protonated. The charged bases were separated by the wide groove of the duplex; this protonation state was defined as the protonation state N4 by Gallego et al. (1999). Two additional simulations were run on both topologies of [d(C2)]4 with the restraints described below, and with charged bases separated by the narrow groove of the duplex. These simulations are referred to as c23-O2 and c25-O2 (Table 1), as the cytosines are now in the protonation state O2 (Gallego et al., 1999).

The molecular dynamics and molecular mechanics calculations were performed using the program AMBER 6.0 (Case et al., 1999), with the parm98 parameter set (Cheatham et al., 1999) and the TIP3P model for water (Jorgensen, 1981). The additional H3 hydrogen of protonated cytosine was of AMBER type H (i.e., an hydrogen bonded to the nitrogen atoms; Cornell et al., 1995). The partial charges of the protonated cytosine were those used by Gallego et al. (1994).

The system was built as described in Malliavin et al. (2003). The thermalization and equilibration protocols for the molecular dynamics (MD) simulations were as described by Young et al. (1997). The atom coordinates were saved each ps. The MD simulations performed with four different initial conditions: [d(C2)]4 with 3′E and 5′E intercalation topologies, and [d(C4)]4 with 3′E and 5′E intercalation topologies, are described in Table 1. Two series were run, either with unrestrained or restrained sugar pucker phases and interphosphate distances. The sugar pucker phases were maintained in the 0–40° range by restraints applied on the five ν_i dihedral angles. The shape of the restraint potential was a well with a square bottom, extended by parabolic sides up to a defined distance or angle value, and then linear sides beyond that. The force constants were set to 30 kcal/mol Å², similar to those used in MD simulations of A-DNA (Cheatham et al., 1997). The interval values for the interphosphate restraints are given in Table 1; for ν_i dihedral angles, the width of the square bottom was 5°, and parabolic sides were used for two subsequent intervals of 5°.

Simulation analysis

The MD simulation analysis was mainly performed with the PTRAJ and AMBER programs (Case et al., 1999). The Visual Molecular Dynamics (VMD; Humphrey et al., 1996) program was used for the visualization of the

TABLE 1   Parameters of the different molecular dynamics (MD) simulations

Simulation id	Solute	Topology	Length (ns)	Water box size (Å)	Number of waters	Pucker restraint	Phosphate restraint (Å)	Charges separation
c23-free	[d(C2)]4	3′E	4	40, 31, 28	881	no	no	*W*
c25-free	[d(C2)]4	5′E	4	40, 33, 28	958	no	no	*W*
c23-3 endo	[d(C2)]4	3′E	2	40, 31, 28	881	N-type	3, 4, 7, 8	*W*
c25-3 endo	[d(C2)]4	5′E	2	40, 33, 28	958	N-type	3, 4, 8, 9	*W*
c43-free	[d(C4)]4	3′E	2	48, 46, 35	2041	no	no	*W*
c45-free	[d(C4)]4	5′E	2	48, 46, 35	2069	no	no	*W*
c43-3 endo	[d(C4)]4	3′E	2	48, 46, 35	2041	N-type	3, 4, 7, 8	*W*
c45-3 endo	[d(C4)]4	5′E	2	48, 46, 35	2069	N-type	3, 4, 8, 9	*W*
c23-O2	[d(C2)]4	3′E	2	40, 31, 28	881	N-type	3, 4, 7, 8	*N*
c25-O2	[d(C2)]4	5′E	2	40, 33, 28	958	N-type	3, 4, 8, 9	*N*

The N-type restraint is a series of harmonic restraints applied to the ribose dihedral angles ν_i to restrain the pucker phase in the 0–40° range. The harmonic restraints on the angles ν_i and on the interphosphate distances were applied using the same potential. The shape of the restraint potential is a well with a square bottom, parabolic sides out to a defined distance or angle value, and then linear sides beyond that. The parameters defining the interphosphate restraints are given in the following order: the upper and lower bounds of the square bottom interval are in the middle; the interval limits for the parabolic sides are on each side. The protonated cytidines of the stacked pairs are separated either by the wide groove (*W*) or by the narrow groove (*N*).

trajectories. The DNA helicoidal parameters were measured from MD snapshots using CURVES 6.0 (Lavery and Sklenar, 1989).

The free energy of the snapshots selected during the simulated trajectories was calculated using the Molecular Mechanics Generalized Born (MMGB) and the Molecular Mechanics Poisson Boltzmann (MMPB) approaches (Massova and Kollman, 1999; Srinivasan et al., 1998). The internal energy of the solute was calculated as its energy in the gas phase. The implicit solvation energy was calculated using the Generalized Born (GB) and the Poisson-Boltzmann (PB) approaches. In both cases, the dielectric constant was set to 1.0 for the molecule interior, and to 80.0 for the solvent. The GB approach (Bashford and Case, 2000) was based on the parameters derived for AMBER (Jayaram et al., 1998). The Born radius of the H3 atom was set to 0.6 Å.

The Poisson-Boltzmann (PB) calculations were run with a temperature of 273 K, using MEAD 1.1.8 (Dillet et al., 1998), and a solvent probe radius of 1.4 Å. The number of points for the finite difference method used in the PB calculation was 101, with a grid spacing of 0.25 Å. Other grids with the numbers of points ranging from 81 up to 121 were tried, and we found that the PB solvation energy was constant between 101 and 121. The PB calculations were performed using a van der Waals radius of 1.1 Å for the hydrogen H3 of protonated cytosine.

For the GB and PB calculations, we used the set of charges derived by Massova and Kollman (1999). The partial charge of H3 was set to 0.4481 to produce the total charge of a protonated cytosine equal to 1, while keeping the charges for the other cytosine atoms equal to those of Massova and Kollman (1999).

The solute hydrophobic energy was calculated as the sum of products of solvent-accessible surface area by atomic solvation parameters (Eisenberg and McLachlan, 1986). The solvent-accessible surface area was calculated using the MSMS 2.5.3 (Sanner et al., 1996) program with a water probe radius equal to 1.4 Å.

The conformational entropy of the solute during the MD simulations was estimated using the approach proposed by Schlitter (1993). A covariance matrix σ of the atomic motions was built from all the extracted snapshots:

$$\sigma_{ij} = \langle (x_i - \langle x_i \rangle)(x_j - \langle x_j \rangle) \rangle, \tag{1}$$

where x_i is the ith atom coordinate and $\langle \rangle$ stands for the mean value. The matrix was then diagonalized, and its eigenvalues were used to calculated an upper bound of the conformational entropy:

$$S' = 0.5k \ln \left(\det \left[Id + \frac{kTe^2}{\hbar^2} M\sigma \right] \right), \tag{2}$$

where Id is the identity matrix, M is the diagonal mass matrix, k is the Boltzmann constant, T the temperature, and $\hbar$ the Planck constant. This method provides only an upper bound of the conformational entropy, but does not require the assumption of a quadratic form of the potential energy surface, and can be thus applied to snapshots extracted from a MD simulation without prior minimization.

After the coordinates of the conformers were stabilized, the snapshots were collected every ps in the 1–4 ns time interval for the c23-free and c25-free simulations, and every ps in the 1–2 ns time interval for the c23-3 endo, c25-3 endo, c43-free, c45-free, c43-3 endo, and c45-3 endo simulations. Geometrical parameters, free energy, conformational entropy, and $\Delta\sigma$ parameters were calculated from all the snapshots, and PB solvation energy for snapshots extracted every 4 ps.

The error on the calculated energy and entropy components was estimated as the standard error on the mean value (Dodge, 1993). Since the total number of the possible conformations of the solute is large with respect to the size of the analyzed conformational sample, the standard error on the mean value can be thus calculated as $S/\sqrt{n}$, where S is the standard deviation of sample.

RESULTS

Conformations of the i-motif during the simulations

During all the MD simulations, the temperature and the system total energy are stable, and the conformers exhibit root-mean-square deviation (RMSD) values from the starting conformer smaller than 2 Å. After a few hundred ps of simulation, the RMSD value reaches a plateau, indicating that the simulations are stabilized after the first nanosecond.

The unrestrained simulations c23-free, c25-free, c43-free, and c45-free displayed a structural shift with respect to the structural i-motif features (Malliavin et al., 2003). First, the phases of sugar pucker (Altona and Sundaralingan, 1972) were found in the 150°–200° range, which is in disagreement with the N-type experimental value (Gehring et al., 1993). The tendency to push the sugar pucker values toward the S-type values is a well-known feature (Cheatham and Kollman, 1996) of the AMBER force fields. Second, several interproton distances established through the measurement of nuclear Overhauser effects (NOEs) were violated, such as the intrastrand restraints between H3′ (ribose) and H6 (base)

and the interstrand restraints between ribose hydrogens H1′, H4′, H2′, and H2″ across the narrow groove. The sugar pucker phases and the interphosphate distances were therefore enforced as described in Materials and Methods, to maintain during the MD simulation, conformers consistent with the x-ray [d(C4)]4 and the NMR [d(C2)]4 structures. As it was shown previously (Malliavin et al., 2003), the simulation run with restraints on the pucker phases and no restraints on the interphosphate distances displays violated interproton distances between the ribose hydrogens across the narrow groove. Restraints on both sugar puckers and interphosphate distances are thus required to minimize the number of violated NMR restraints.

The conformations sampled during both c23-3 endo and c23-O2 molecular dynamics simulations are in good agreement with the NMR measurements performed on [d(C2)]4. Both exhibit four distance violations of the NMR restraints in the 0.8–1 Å range. The NOE violations in c23-O2 only involve intersugar restraints across the narrow groove, whereas in the c23-3 endo simulation, the NOE violations also involve ribose-base restraints.

The helicoidal parameters were calculated for each intercalated duplex. The helical twist and the rise exhibit the largest variations along the MD trajectories (Malliavin et al., 2003). The c23-free and the c25-free duplexes display large heterogeneity of the rise and twist values, indicating poor conformational fit of the phosphodiester backbones and poor base intercalation. The c23-free, c25-free, and c25-3 endo mean conformers display rise and twist values different from those observed in the NMR structure of [d(C2)]4, whereas the c23-3 endo mean conformer and the conformers obtained from the trajectories run on the [d(C4)]4 tetramer have rise and twist values closer to those measured in the x-ray and NMR structures. A conformational analysis of the conformers generated by the MD simulations shows that those with the largest rise values (rise ≥ 6.5 Å) exhibit unfavorable stacking and ion-dipole interaction which is not balanced by the small reduction of the repulsion between the charged H3 hydrogens. This is the case for the c25-3 endo conformer whose rise, 6.94 Å, is 0.5 Å larger than that of the corresponding c23-3 endo conformer. The observation of a larger rise for the c25-3 endo may account for the experimental observation (Leroy et al., 2001) of a better stability for the 3′E topology of [d(C2)]4.

The variation of the helical twist of each duplex of [d(C2)]4 was monitored (Fig. 2) in the 1–2 ns interval along the MD trajectories. The unrestrained simulations performed on [d(C2)]4 (c23-free and c25-free simulations) show a better fit of the intercalated duplexes to the crystallographic structure in the case of the 5′E topology. Indeed, Fig. 2, a and b, shows that the fluctuations of the twist of each duplex seem to be connected with the fluctuations of the twist of the other duplex in the case of c25-free, and that the twist fluctuations in both duplexes seem to be independent in the case of c23-free. This behavior is paradoxical with
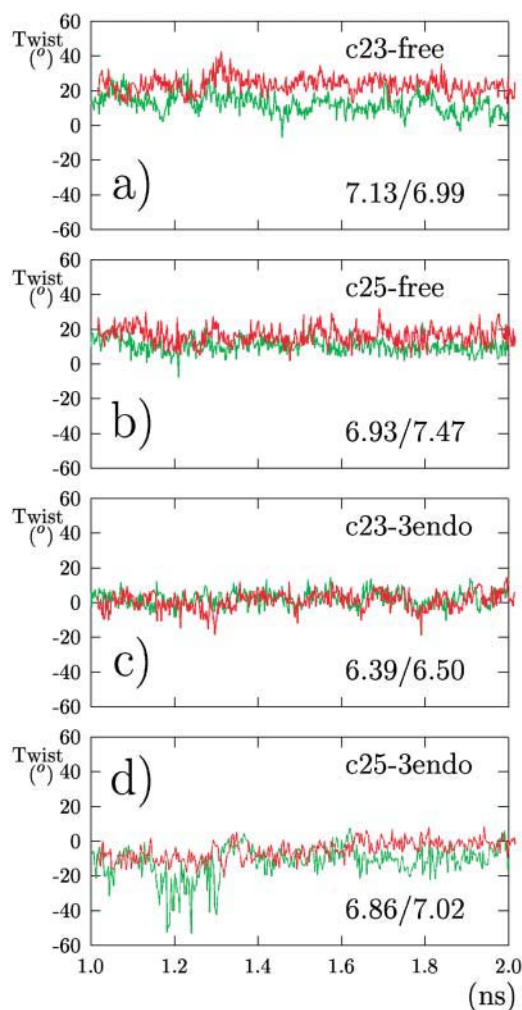

FIGURE 2   Mean helical twist values (Å) calculated on each duplex of the i-motif and displayed along the trajectories: c23-free (*a*), c25-free (*b*), c23-3 endo (*c*), and c25-3 endo (*d*). The twist of one duplex is shown in green line, the twist of the other in red line. The mean rise value, Å, of each duplex is also given.

respect to the smaller number of sugar-sugar interactions between phosphodiester backbones in c25-free than in c23-free, and suggests that the phosphodiester backbone undergoes larger steric hindrance in the case of two sugar-sugar interactions. For the restrained simulations performed on [d(C4)]4, the fluctuations of the twist in the 3′E topology are nearly superimposed (Fig. 2 *c*). By contrast, Fig. 2 *d* shows that one duplex in the 5′E topology displays transiently large flexibility in the 1.15–1.25 ns interval, which is a sign of a reduced stability of the tetramer. The restraints applied on sugar pucker and on the interphosphate distances are thus sufficient to produce a good fit between the backbones in the case of 3′E topology, but not in the case of 5′E topology.

Relative energies and mobilities

For each topology, the mean values and the standard error $s = S/\sqrt{n}$ of the energy components and of S′, the upper

TABLE 2 Values of the free energy components

Simulation id	Elect*	VdW[†]	Internal[‡]	Nonpolar[§]	Solvation (GB)[¶]	Total[‖]	Solvation (PB)**	S′ value[††]	Restraint[‡‡]	Δ twist[§§] value (°)
c23-3 endo	−2530 (0.5)	−31 (0.2)	346 (0.4)	9.5 (0.003)	−363 (0.3)	−2568	−400 (0.5)	183 (0.05)	5 (0.06)	–
c25-3 endo	−2543 (0.5)	−20 (0.2)	353 (0.3)	9.8 (0.03)	−347 (0.3)	−2547	−392 (0.7)	199 (0.4)	4 (0.05)	–
Diff. 3–5	13, 0.25%	−11, 21%	−7, 1.0%	−0.3, 1.5%	−16, 2.2%	−21	−8, 1.0%	−16, 4.2%	1, 11%	8.15
c23-O2	−2548 (0.5)	−28 (0.2)	351 (0.4)	9.5 (0.003)	−363 (0.3)	−2578	–	243 (0.1)	4.3 (0.05)	–
c25-O2	−2525 (0.5)	−22 (0.2)	353 (0.4)	9.7 (0.004)	−377 (0.3)	−2560	–	257 (0.05)	4.2 (0.05)	–
Diff. 3–5	−23, 0.45%	−6, 12%	−2, 0.28%	−0.2, 1.0%	14, 1.9%	−18	–	−14, 2.8%	0.1, 1.6%	9.0
c43-3 endo	−5043 (0.8)	−101 (0.3)	716 (0.5)	16 (0.003)	−1749 (0.6)	−6161	−1798 (1.2)	213 (0.3)	12 (0.095)	–
c45-3 endo	−5018 (1.0)	−90 (0.3)	731 (0.5)	15 (0.003)	−1743 (0.7)	−6105	−1789 (1.4)	161 (0.3)	14 (0.1)	–
Diff. 3–5	−25, 0.25%	−11, 6%	−15, 1.0%	1, 3.2%	−6, 0.17%	−56	−9, 0.25%	52, 14%	−2, 7.5%	5.79

The mean energy and conformational entropy, S′, values are shown together with the standard error $s = S/\sqrt{n}$ in parentheses. The energies (kcal/mol) and the S′ values (cal/(mol K)) are computed for each MD simulation. The differences $E^{3'E} - E^{5'E}$ of each energy or entropy component between the 3′E and the 5′E topology are given together with the ratio $\delta\% = (E^{3'E} - E^{5'E})/(E^{3'E} + E^{5'E})$ expressed as a percentage. The difference of mean twist values between 3′E and 5′E topologies is also given.

*Coulombic electrostatic energy E_{coul}.

[†]Lennard-Jones energy E_{LJ}.

[‡]Internal energy $E_{int} = E_{bnd} + E_{ang} + E_{dih}$ where E_{bnd} is the bond harmonic energy, E_{ang} the angle harmonic energy, and E_{dih} the dihedral angle energy.

[§]Hydrophobic solvation energy E_{hyd}, calculated from the solvent accessible surfaces (Eisenberg and McLachlan, 1986).

[¶]Solvation energy E_{GB} calculated using the Born generalized model (Srinivasan et al., 1998).

[‖]Total energy $E_{tot} = E_{int} + E_{coul} + E_{LJ} + E_{hyd} + E_{GB}$.

**Solvation energy E_{PB} calculated by solving the Poisson-Boltzmann equation (Dillet et al., 1998).

[††]The upper bound S′ of the conformational entropy (Schlitter, 1993).

[‡‡]The restraint energy, obtained from the restraint potential applied on sugar pucker phases and interphosphate distances.

[§§]The difference of mean helical twist values between the simulations run in 3′E and 5′E topologies.

bound of the conformational entropy, calculated as described in Materials and Methods, are displayed in Table 2, together with the differences between the 3′E and 5′ topologies (Difference 3–5). The observation that the values of the standard deviation S calculated from each 200 ps subset of the trajectories are of the same order of value as the standard deviations calculated from the complete trajectories reflects the convergence of the calculated energy components in the considered simulation length. As the conformers obtained during the restrained simulations were in better agreement with the experimental observations, the energetic analysis was performed only on these simulations.

The values of the restraint energy produced by applying restraints on the ribose pucker and on the interphosphate distances are the smallest energy components. The differences of restraint energy between the two topologies, <2 kcal/mol, are smaller than the energy fluctuations during the MD trajectories. Hence their contribution can be neglected in the analyses.

For each energy component, the differences between the 3′E and 5′E topologies can be analyzed with the ratio: $\delta\% = (E^{3'E} - E^{5'E})/(E^{3'E} + E^{5'E})$, where $E^{3'E}$ and $E^{5'E}$ are the energies of the 3′E and 5′ topologies (Table 2). The $\delta\%$ values measured are always <12%, except in the case of the c23-3 endo/c25-3 endo simulations, which show that the van der Waals energy is more favorable (21%) for the 3′E topology. The comparison of the c23-3 endo/c25-3 endo, c23-O2/c25-O2, and c43-3 endo/c45-3 endo simulation pairs shows that the percentage difference for the van der Waals energy increases with the differences of mean helical twist (Δ

twist) between two simulations run with different topologies (Table 2). The difference of van der Waals energy between the two topologies is thus directly related to the twist of the phosphodiester backbones.

The electrostatic energy component of [d(C2)]4 advantages the 5′E topology with respect to the 3′E topology. This is in agreement with the observation (Leroy et al., 2001) that a pair of close phosphate groups is transformed into a pair of remote phosphate groups when the intercalation is changed from 3′E to 5′E. But, for the c23-O2/c25-O2 and c43-3 endo/c45-3 endo simulation pairs, the 3′E topology is advantaged by the electrostatic energy. The structural basis for the electrostatic energy value was thus further analyzed by calculating the middle of the interphosphate distances between the close and remote phosphate pairs across the narrow groove (Table 3). For the c23-3 endo/c23-3 endo and c43-3 endo/c43-3 endo simulation pairs, the most favorable electrostatic energy is obtained for the topology displaying the largest interphosphate distances, and thus the smallest repulsion. For the c23-O2/c25-O2 simulation pair, this is not the case, and the difference of electrostatic energy is thus coming from another source than the phosphate interaction. In any case, the small electrostatic differences ($\delta\%$) between the 3′E and 5′E topologies (Table 2), show that the electrostatic contribution is not the dominant one.

The energy components calculated for the c23-O2 simulation (Table 2) shows some differences with those calculated for the c23-3 endo simulation. The Coulombic electrostatic component is more negative in c23-O2 than in c23-3 endo, which is in agreement with the observations of

TABLE 3 Interphosphate distance values observed during the MD simulations

Simulation id	Close P-P pairs (Å)	Remote P-P pairs (Å)
c23-3 endo	6.8 (0.2)	–
c25-3 endo	–	7.85 (0.1)
c23-O2	6.8 (0.4)	–
c25-O2	–	7.5 (0.5)
c43-3 endo	7.0 (0.2)	9.1 (0.6)
c45-3 endo	6.55 (1.3)	8.0 (0.2)

For each simulation, mean interphosphate distance across the narrow groove were sorted as remote distances for phosphorus pairs belonging to cytidines stacked by their faces oriented toward the 3′E end, and sorted as close distances for phosphorus pairs belonging to cytidines stacked by their faces oriented toward the 5′ end (Fig. 1). The middle values of the phosphorus (P-P) distances are displayed, and the amplitudes of the phosphorus distance fluctuations during the MD simulation are given in parentheses. In [d(C2)]4, a single close or remote interphosphate distance is encountered, according to the 3′E or 5′E topology.

Gallego et al. (1999), and is coming from the less repulsive electrostatic stacking interaction between O2 steps.

Although the crystal structure of d(CCCC)4 is observed with the 5′E intercalation topology, the 3′E conformation of d(CCCC) is here favored by the electrostatic and van der Waals energy terms. This paradox can be explained in two ways. First, the preference of [d(C4)]4 for the 5′E topology in the crystal is not observed in solution, where both topologies have similar stabilities (Leroy et al., 2001). Second, in the crystal, the packing effects can explain the better stability of the 5′E topology, and these effects are not considered in the simulations presented here.

For the simulations c23-3 endo, c25-3 endo, c43-3 endo, and c45-3 endo, the Poisson-Boltzmann (PB) and Generalized Born (GB) solvation energies differ by ~45 kcal/mol. Both sets of solvation energies were compared by linear regression analysis with XMGR (Grace Development Team, 2000); the slope and intercept values of 1.00 and −33.16 kcal/mol were found. The offset of the PB and GB energies is not a problem here, since we just consider the free energy differences between the 3′E and 5′E intercalation topologies. As equivalent results were obtained for PB and GB solvation energies for c23-3 endo, c25-3 endo, c43-3 endo, and c45-3 endo, the PB calculations were not performed in the case of c23-O2/c25-O2.

As S′ is only an upper bound of the conformational entropy, it is difficult to relate the difference of S′ observed between the 3′E and 5′E topologies to concrete conformational changes. Nevertheless, the S′ values obtained here are decreasing for increasing values of the restraint energy, which is in agreement with the definition of S′ (Eq. 2). The large S′ values obtained for c25-3 endo can be related to the large twist fluctuations observed along its MD trajectory (Fig. 2 d).

The atomic fluctuations (Fig. 3) are in certain correlation with the S′ values. Indeed, they are larger for c25-3 endo than for c23-3 endo (Fig. 3 a), which is in agreement with the
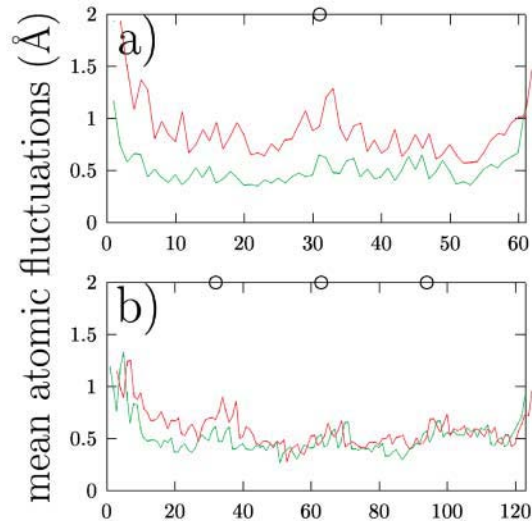

FIGURE 3 Mean atomic fluctuations (Å) calculated over all the trajectories, shown with respect to the atom name, for the simulations run on [d(C2)]4 (a) and on [d(C4)]4 (b) with restraints. The atomic fluctuations of each atom are calculated as the mean value of its atomic fluctuations on the four strands. The fluctuations were computed for the 3′ (green lines) and 5′E (red lines) topologies. The unfilled circles indicate the phosphorus positions along the sequence.

larger fluctuations of the helical twist (Fig. 2 d) obtained for c25-3 endo. Similar results are obtained for c23-O2 and c25-O2 (conformational entropies: Table 2, atomic fluctuations: data not shown). But, the difference of S′ values obtained for the c43-3 endo/c45-3 endo (Fig. 3 b) simulation pair is in disagreement with the difference in atomic fluctuations, as both topologies display similar fluctuations whereas the 5′E topology displays a smaller S′ value than the 3′E topology.

Along the unrestrained (respectively restrained) MD trajectories, the N3–H3 distance fluctuations are in the 1.87–1.95 Å (respectively 1.91–2.10 Å) ranges, and (N3, H3, N3) angles are in the 158–166° (respectively 156–164°) ranges. All these intervals are consistent with the formation of hydrogen bonds. Slightly larger N3–H3 distances and smaller (N3, H3, N3) angles are obtained for restrained simulations. The (N3, H3, N3) angle values are slightly smaller than those calculated with ab initio methods (Spóner et al., 1996). A single N3...H3 distance inconsistent with hydrogen bond formation was observed along the c25-3 endo and c45-3 endo simulation trajectories, in the 700–800 ps, and in the 150–250 ps intervals. Apart from these two isolated events, the cytosine base pairs are stable during the simulations.

The interactions between the phosphodiester backbones

Among all the energy differences calculated between the 3′E and 5′E topologies (Table 2), the largest differences (δ%) of energy are observed for the van der Waals energy com-

ponents. To relate this observation to conformational properties, the solvent-accessible surfaces of atoms in the two topologies were compared. Indeed, the water accessibility of an atom is directly related to its ability to establish van der Waals interactions with other atoms of the solute.

The solvent-accessible surface area S_{ik} of all the atoms i in each residue k was calculated as described in Materials and Methods. The MD simulations performed with $3'E$ and $5'E$ topologies were then compared by calculating, for each atom i of the i-motif, the parameter $\Delta\sigma_i$, which is the mean sum on all the residues k, of the difference of solvent-accessible surface areas $S_{ik}^{3'E}$ and $S_{ik}^{5'E}$ of the atom i in both topologies,

$$\Delta\sigma_i = \left\langle \sum_k (S_{ik}^{3'E} - S_{ik}^{5'E}) \right\rangle, \tag{3}$$

where $\langle \ \rangle$ is the mean value calculated on all the residues k and over the considered snapshots. Four sets of $\Delta\sigma_i$ values were calculated on each couple of trajectories (c23-free/c25-free, c23-3 endo/c25-3 endo, c43-free/c45-free and c43-3

endo/c45-3 endo) by comparing two-by-two the snapshots having the same rank in the two simulations (Fig. 4).

The parameters $\Delta\sigma_i$ represent the accessibility difference of the atom i in the $3'E$ and $5'E$ topologies. Negative $\Delta\sigma_i$ values indicate a reduced accessibility to water in the $3'E$ topology and an increase of the potential van der Waals interaction.

The four sets of $\Delta\sigma_i$ values, corresponding to the comparison of the c23-free/c25-free pair (Fig. 4 a), of the c43-free/c45-free pair (Fig. 4 b), and of the corresponding restrained simulations (Fig. 4 c), are displayed. In all the analyses, the $\Delta\sigma_i$ and the standard deviation values, obtained for the atoms belonging to the bases, show that these $\Delta\sigma_i$ values are not significantly different from zero. This is in agreement with the axial symmetry of the i-motif structure (Gehring et al., 1993). $\Delta\sigma_i$ values, significantly different from zero, are obtained for the atoms belonging to the phosphodiester backbone. These values mainly arise from the different positions of end residues in the two topologies, as the residues located in the center of the i-motif structure
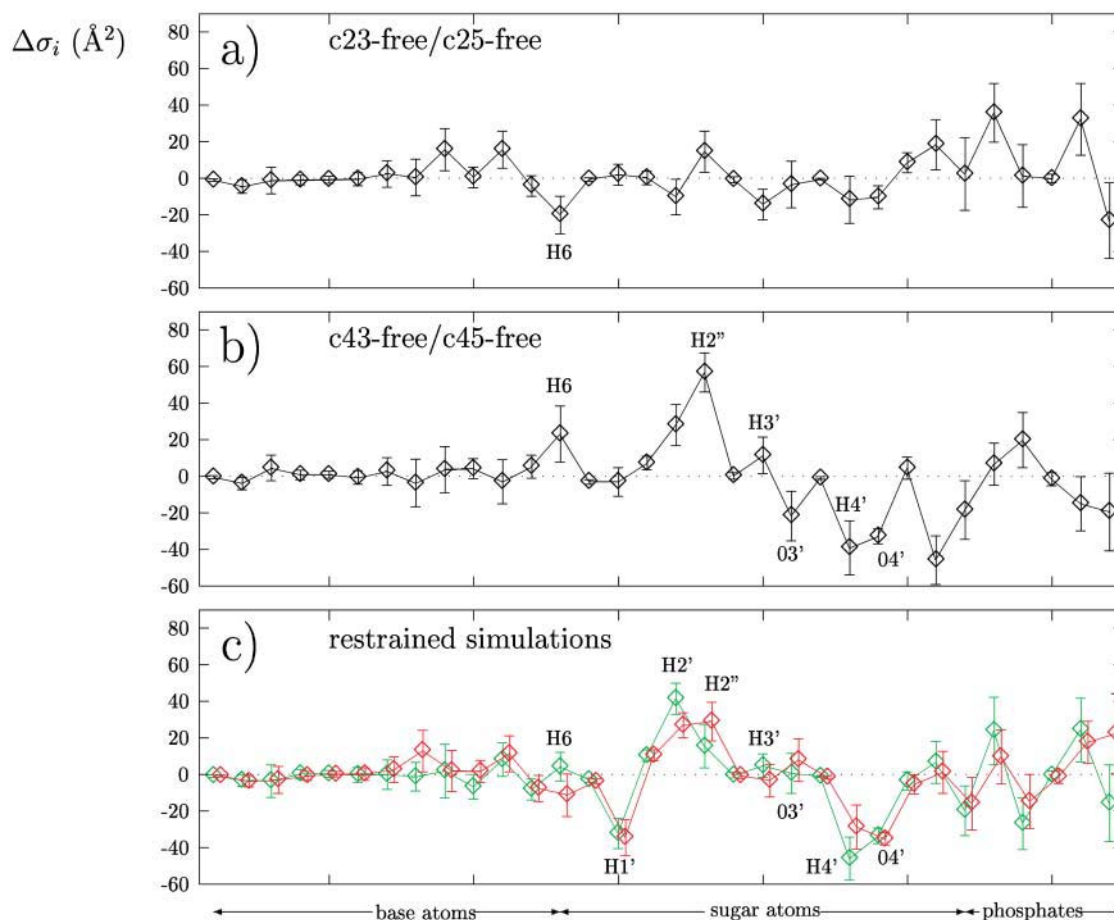

FIGURE 4 The $\Delta\sigma_i$ values describing the difference of the atom surface accessibility in the $3'E$ and $5'E$ topologies (Å^2) and their standard deviations. Negative values indicate a better accessibility in the $5'E$ topology. The $\Delta\sigma_i$ values are displayed for the unrestrained simulations c23-free/c25-free run on [d(C2)]4 (a), for the unrestrained simulations c43-free/c45-free run on [d(C4)]4 (b), and for the restrained simulations run on [d(C2)]4 (c, *green line*, c23-3 endo/c25-3 endo) and [d(C4)]4 (c, *red line*, c43-3 endo/c45-3 endo). The regions corresponding to bases, to sugars and to phosphate groups are indicated. The simulations performed with the sugar restrained in the $3'$ endo conformation show: i), a better accessibility of the H2'/H2" in the $3'E$ topology; and ii), a better accessibility of H1'/H4'/O4' in the $5'E$ topology.

do not experience large environment change in the two topologies.

The $\Delta\sigma_i$ values obtained for the sugar atoms display a flatter pattern for the c23-free/c25-free pair (Fig. 4 *a*) than for the other pairs; indeed, they are in the $-20/20$ Å^2 range in Fig. 4 *a* and in the $-60/60$ Å^2 range in Fig. 4, *b* and *c*. The small differences observed for c23-free/c25-free between the atom accessibilities are the sign of weak van der Waals interactions between the backbones. This weak interaction can be explained by the helical twist heterogeneity and the poor fit between the conformations of the phosphodiester backbones (Fig. 2, *a* and *b*).

The series of $\Delta\sigma_i$ values calculated for the two pairs of restrained simulations (Fig. 4 *c*) display very similar shapes, and the differences between them are in the range of their standard deviations. This is not surprising, as equivalent sets of restraints were applied on the phosphodiester backbones.

The largest $\Delta\sigma_i$ values are observed for atoms H2″, H4′, and O4′ in the c43-free/c45-free comparison (Fig. 4 *b*), and for atoms H1′, H2′, H2″, H4′, and O4′ for the restrained simulations (Fig. 4 *c*). Among these atoms, H1′, O4′, and H4′ display negative $\Delta\sigma_i$ values, indicating lesser accessibility in the 3′E topology and possible van der Waals contacts with other i-motif atoms. This can be related to the observations made on the x-ray crystallographic structure of [d(C4)]4 (Berger et al., 1996), that the relative positions of atoms O4′, C4′, and C1′ of neighboring sugars are consistent with the existence of CH...O hydrogen bonds. Furthermore, Gallego et al. (1999) pointed out the importance of van der Waals interactions between the sugar-phosphate backbones.

The sums of the $\Delta\sigma_i$ values calculated for the sugar atoms are -43.9 Å^2 for c23-3 endo/c25-3 endo and -33.7 Å^2 for c43-3 endo/c45-3 endo. These negative values, which indicate larger accessibilities for the 5′E topology, are consistent with the de-favorable van der Waals energy in the 5′E topology (Table 2). Moreover, the larger the percentage energy difference, the larger is the absolute value of the sum of $\Delta\sigma_i$. This suggests that the $\Delta\sigma_i$ differences reflect the loss of one sugar-sugar van der Waals interaction between 3′E and 5′E topologies.

The $\Delta\sigma_i$ values calculated for the pair c23-O2/c25-O2 (data not shown) display features similar to those obtained for the pair c23-3 endo/c25-3 endo.

For each couple of neighboring sugars, the four possible C4–H4′...O4′ and C1–H1′...O4′ mean distances and the C–H...O4′ angles were calculated along the trajectories, and only the smallest mean distance is further considered. Almost all the 40 mean distance and angle values are clustering ~2.8 Å and 125°, close to the mean distance and angle values (2.4 Å, 131°) measured in the x-ray crystallographic structure of [d(C4)]4 (Berger et al., 1996). They are also in agreement with the values obtained from a statistical analysis of organic crystal structures (Taylor and Kennard, 1982) and of membrane protein structures (Senes et al., 2001).

The mean CH...O distance calculated from restrained

trajectories is slightly smaller (2.8 Å) and closer to x-ray distances than the mean CH...O distance value (3.0 Å) calculated from unrestrained trajectories. This small difference allows one to neglect the influence of the restraints on the lengths of CH...O distances.

The mean value of H1′...O4′ distances (1.8 Å) is smaller than the mean value of H4′...O4′ distances (3.0 Å). These smaller H1′...O4′ distances indicate better interaction between atoms in the C1H1′...O4′ pairs than in the C4′H4′...O4′ ones. On the other hand, more close H4′...O4′ pairs are observed in restrained (seven pairs) than in unrestrained (three pairs) simulations. One effect of the N-type sugar pucker, present in restrained simulations and experimentally observed (Gehring et al., 1993), seems thus to slightly advantage the CH1′...O4′ interactions over the CH4′...O4′ ones, and as seen above, to induce a better interaction between the sugars.

DISCUSSION AND CONCLUSION

The two topologies of the i-motif structure were compared by MD simulations. The differences observed are mainly related to the conformation of the phosphodiester backbone, either with regard to the sugar pucker phase, or to the helical twist.

The stability of the B-DNA duplex is mainly due to a favorable stacking of consecutive covalently linked bases, corresponding to an attractive Lennard-Jones contribution to the energy in the range of -17.96 to -19.47 Kcal/mol (Friedman and Honig, 1992). The correct helical twist of the B-DNA structures can be predicted in the frame of a spring model for the backbone (Tung and Harvey, 1984), with constants from 0.016 to 0.021 kcal/(mol/deg^2). In the duplex, the energy required to twist the backbone (~6 kcal/mol for a twist value of 30°) is thus small with respect to the base stacking energy, and the twist of the phosphodiester backbone is mainly determined by the rise between the bases. An analysis of the helicoidal parameters of DNA-intercalator structures (PDB ids: 108d, Spielmann et al., 1995; 1c9z, Shui et al., 2000; 1dsc, Lian et al., 1996; 145d, Peek et al., 1994; 1d32, Gao et al., 1991) shows twist values in the 7–25° range for bases involved in intercalation, and having thus large rise values, and twist values in the 26–40° range for other bases.

An increase of the rise destabilizes a i-motif tetramer more than a Watson-Crick duplex of equivalent size, because of the presence of the charged C-imino protons. Indeed, the mean conformers of c23-free, c25-free, and c25-3 endo, which display rise values larger than 6.8 Å, exhibit also heterogeneous or very negative twist values (Fig. 2). Consequently, the twisting of the phosphodiester backbone, which induces the value of the rise, is critical for the i-motif stability, and therefore all the phosphodiester backbones should display the same twist, to produce a good stacking of bases.

To keep the backbone twisting at the same value for

the four DNA strands, an attractive interaction between the strands is certainly required. In the frame of the model quoted above (Tung and Harvey, 1984), the required energy, for a twist value of ~10°, can be evaluated to be ~1.6–2.1 kcal/mol, per strand and per base. The free energy calculations presented here (Table 2) show that in percentage, the largest energy difference which advantages the 3′E with respect to the 5′E topology in [d(C2)]4 is the van der Waals energy component. An analysis of atom relative accessibilities (Fig. 4) demonstrates that the largest accessibility difference between the two topologies involves the atoms of the sugar moieties. An attractive interaction between sugars, whatever one calls its origin (van der Waals, Gallego et al., 1999; or CH...O hydrogen bonds, Berger et al., 1996), is thus responsible for the correct backbone twisting. The N-type sugars permit shorter CH...O distances, and thus better sugar-sugar interactions.

This model can also explain, in the case of [d(C2)]4, the greater stability of the 3′E topology with respect to the 5′E topology. Indeed, as quoted above, the phosphodiester backbone twisting requires an energy of 1.6 kcal/mol, and the positive interaction between the sugars was measured to be 0.6 kcal/mol (Leroy et al., 2001). This indicates that about two positive sugar-sugar interactions are sufficient to balance the twisting energy. For [d(C2)]4 in 5′E topology, the number of favorable interactions, one for each backbone pair, is not sufficient to produce good base stacking. Thus, the 5′E topology is unstable and not observed experimentally.

REFERENCES

Ahmed, S., A. Kintanar, and E. Henderson. 1994. Human telomeric C-strand tetraplexes. *Nat. Struct. Biol.* 1:83–88.

Altona, C., and M. Sundaralingam. 1972. Conformational analysis of the sugar ring in nucleosides and nucleotides. A new description using the concept of pseudorotation. *J. Am. Chem. Soc.* 94:8205–8212.

Arthanari, H., and P. Bolton. 2001. Functional and dysfunctional roles of quadruplex DNA in cells. *Chem. Biol.* 8:221–239.

Bashford, D., and D. Case. 2000. Generalized Born models of macromolecular solvation effects. *Annu. Rev. Phys. Chem.* 51:129–152.

Berger, I., M. Egli, and A. Rich. 1996. Inter-strand C=H=O hydrogen bonds stabilizing four-stranded intercalated molecules: stereoelectronic effects of O4′ in cytosine-rich DNA. *Proc. Natl. Acad. Sci. USA.* 93:12116–12121.

Case, D., D. A. Pearlman, J. W. Caldwell, T. E. Cheatham, W. Ross, C. Simmerling, T. Darden, K. Merz, R. Stanton, A. Cheng, J. Vincent, M. Crowley, V. Tsui, R. Radmer, Y. Duan, J. Pitera, I. Massova, G. Seibel, U. Singh, P. Weiner, and P. Kollman. 1999. AMBER6.

Cheatham, T. E., P. Cieplak, and P. Kollman. 1999. A modified version of the Cornell et al. force field with improved sugar pucker phases and helical repeat. *J. Biomol. Struct. Dyn.* 16:845–861.

Cheatham, T. E., M. Crowley, T. Fox, and P. Kollman. 1997. A molecular level picture of the stabilization of A-DNA in mixed ethanol-water solutions. *Proc. Natl. Acad. Sci. USA.* 94:9626–9630.

Cheatham, T. E., and P. Kollman. 1996. Observation of the A-DNA to B-DNA transition during unrestrained molecular dynamics in aqueous solution. *J. Mol. Biol.* 259:434–444.

Chen, L., L. Cai, X. Zhang, and A. Rich. 1994. Crystal structure of a four-stranded intercalated DNA: d(C4). *Biochemistry.* 33:13540–13546.

Cornell, W., P. Cieplak, C. Bayly, I. Gould, K. Merz, D. Ferguson, D. Spellmeyer, T. Fox, J. Cadwell, and P. Kollman. 1995. A second generation force field for the simulation of proteins, nucleic acids, and organic molecules. *J. Am. Chem. Soc.* 117:5179–5197.

Dillet, V., H. Dyson, and D. Bashford. 1998. Calculations of electrostatic interactions and pK_as in the active site of *Escherichia coli* thioredoxin. *Biochemistry.* 37:10298–10306.

Dodge, Y. 1993. Statistique: Dictionnaire Encyclopédique. Dunod, Paris.

Eisenberg, D., and A. McLachlan. 1986. Solvation energy in protein folding and binding. *Nature.* 319:199–203.

Friedman, R., and B. Honig. 1992. The electrostatic contribution to DNA base-stacking interactions. *Biopolymers.* 32:145–159.

Gallego, J., E. Golden, D. Stanley, and B. Reid. 1999. The folding of centromeric DNA strands into intercalated structures: a physicochemical and computational study. *J. Mol. Biol.* 285:1039–1052.

Gallego, J., F. Luque, M. Orozco, and F. Gago. 1994. Binding of echinomycin to d(GCGC)2 and d(CCGG)2 distinct stacking interactions dictate the sequence dependent formation of Hoogsteen base pairs. *J. Biomol. Struct. Dyn.* 12:111–129.

Gao, Q., L. Williams, M. Egli, D. Rabinovich, S. L. Chen, G. G. Quigley, and A. Rich. 1991. Drug-induced DNA repair: x-ray structure of a DNA-ditercalinium complex. *Proc. Natl. Acad. Sci. USA.* 88:2422–2426.

Gehring, K., J. L. Leroy, and M. Guéron. 1993. A tetrameric DNA structure with protonated cytosine base pairs. *Nature.* 363:499–500.

Grace Development Team. 2000. Grace-5.1.2. http://plasma-gate.weizmann. ac.il/Grace/.

Guéron, M., and J. L. Leroy. 2000. The i-motif in nucleic acids. *Curr. Opin. Struct. Biol.* 10:326–331.

Humphrey, W., A. Dalke, and K. Schulten. 1996. VMD—Visual Molecular Dynamics. *J. Mol. Graph.* 14:33–38.

Jayaram, B., D. Sprous, and D. Beveridge. 1998. Solvation free energy of biomacromolecules: parameters for a modified generalized Born model consistent with the Amber force field. *J. Phys. Chem. B.* 102:9571–9576.

Jorgensen, W. 1981. Transferable intermolecular potential functions for water, alcohols and ethers. Application to liquid water. *J. Am. Chem. Soc.* 103:335–340.

Keniry, M. 2000. Quadruplex structures in nucleic acids. *Biopolymers.* 56:123–146.

Lavery, R., and H. Sklenar. 1989. The definition of generalized helicoidal parameters and of axis curvature for irregular nucleic acids. *J. Biomol. Struct. Dyn.* 6:63–91.

Leroy, J. L., and M. Guéron. 1995. Solution structures of the i-motif tetramers of d(TCC), d(5methylCCT) and d(T5methylCC): novel NOE connections between amino protons and sugar protons. *Structure.* 3:101–120.

Leroy, J. L., K. Snoussi, and M. Guéron. 2001. Investigation of the energetics of C-H.O hydrogen bonds in the DNA i-motif via the equilibrium between alternative intercalation topologies. *Magn. Res. Chem.* 39:S171–S176.

Lian, C., H. Robinson, and A. J. Wang. 1996. Structure of actinomycin D bound with (GAAGCTTC)2 and (GATGCTTC)2 and its binding to the (CAG)N: (CTG)N triplet sequence by NMR analysis. *J. Am. Chem. Soc.* 118:8791–8801.

Malliavin, T. E., K. Snoussi, and J. L. Leroy. 2003. The NMR structure of $[Xd(C2)]^4$ investigated by molecular dynamics simulations. *Magn. Res. Chem.* 41:18–25.

Massova, I., and P. Kollman. 1999. Computational alanine scanning to probe protein-protein interactions: a novel approach to evaluate binding free energies. *J. Am. Chem. Soc.* 121:8133–8143.

Nonin-Lecomte, S., and J. L. Leroy. 2001. Structure of a C-rich strand fragment of the human centromeric satellite III: a pH-dependent intercalation topology. *J. Mol. Biol.* 309:491–506.

Peek, M., L. Lipscomb, J. Bertrand, Q. Gao, B. Roques, C. Garbay-Jaureguiberry, and L. Williams. 1994. DNA distortion in bis-intercalated complexes. *Biochemistry.* 33:3794–3800.

Phan, A., M. Guéron, and J. L. Leroy. 2000. Intramolecular i-motif structures of telomeric DNA. *J. Mol. Biol.* 299:123–144.

Phan, A., and J. L. Leroy. 2000. An intramolecular i-motif: the solution structure and base-pair opening kinetics of (5mCCT3CCT3ACCT3CC). *J. Biomol. Struct. Dyn.* 299:123–144.

Sanner, M., A. Olson, and J. Spehner. 1996. Reduced surface: an efficient way to compute molecular surfaces. *Biopolymers.* 38:305–320.

Schlitter, J. 1993. Estimation of absolute and relative entropies of macromolecules using the covariance matrix. *Chem. Phys. Lett.* 215: 617–621.

Senes, A., I. Ubarretxena-Belandia, and D. Engelman. 2001. The C α-H.O hydrogen bond: a determinant of stability and specificity in trans-membrane helix interactions. *Proc. Natl. Acad. Sci. USA.* 98:9056–9061.

Shui, X., M. Peek, L. Lipscomb, A. Wilkinson, L. Williams, M. Gao, C. Ogata, B. Roques, and C. Garbay-Jaureguiberry. 2000. Effects of cationic charge on three-dimensional structures of intercalative complexes: structure of a bis-intercalated DNA complex solved by MAD phasing. *Curr. Med. Chem.* 7:59–71.

Spacková, N., I. Berger, M. Egli, and J. Spóner. 1998. Molecular dynamics of hemiprotonated intercalated four-stranded i-DNA: stable trajectories on a nanosecond scale. *J. Am. Chem. Soc.* 120:6147–6151.

Spielmann, H., D. Wemmer, and J. Jacobsen. 1995. Solution structure of a DNA complex with the fluorescent bis-intercalator TOTO determined by NMR spectroscopy. *Biochemistry.* 34:8542–8553.

Spóner, J., J. Leszczynski, V. Vetter, and P. Hobza. 1996. Base stacking and hydrogen bonding in protonated dimer: the role of molecular ion-dipole and induction interactions. *J. Biomol. Struct. Dyn.* 13:695–706.

Srinivasan, J., T. E. Cheatham, P. Cieplak, P. Kollman, and D. Case. 1998. Continuum solvent studies of the stability of RNA hairpin loops and helices. *J. Biomol. Struct. Dyn.* 16:671–682.

Taylor, R., and O. Kennard. 1982. Crystallographic evidence for the existence of C-H.O, C-H.N and C-H. Cl hydrogen bonds. *J. Am. Chem. Soc.* 104:5063–5070.

Tung, C., and S. Harvey. 1984. A molecular mechanical model to predict the helix twist angle of B-DNA. *Nucl. Acid. Res.* 12:3343–3356.

Young, M., G. Ravishanker, and D. Beveridge. 1997. A 5-nanosecond molecular dynamics trajectory for B-DNA: analysis of structure, motions, and solvation. *Biophys. J.* 73:2313–2336.